

## Hollow $\text{In}_2\text{O}_3@\text{ZnFe}_2\text{O}_4$ heterojunctions for highly efficient photocatalytic degradation of tetracycline under visible light

Weihua Fei<sup>a</sup>, Yun Song<sup>a</sup>, Najun Li<sup>\*, a, b</sup>, Dongyun Chen<sup>a, b</sup>, Qingfeng Xu<sup>a, b</sup>, Hua Li<sup>a, b</sup>, Jinghui He<sup>a</sup>, Jianmei Lu<sup>\*, a, b</sup>

<sup>a</sup> College of Chemistry, Chemical Engineering and Materials Science, Collaborative Innovation Center of Suzhou Nano Science and Technology, Soochow University, Suzhou, Jiangsu 215123, China

<sup>b</sup> National Center of International Research on Intelligent New Nanomaterials and Detection Technologies in Environmental Protection, Suzhou, Jiangsu 215123, China

\*Correspondence to: N. J. Li (E-mail: linajun@suda.edu.cn) & J. M. Lu (E-mail: lujm@suda.edu.cn), Tel/Fax: 86 512 65880367

### Supporting Information

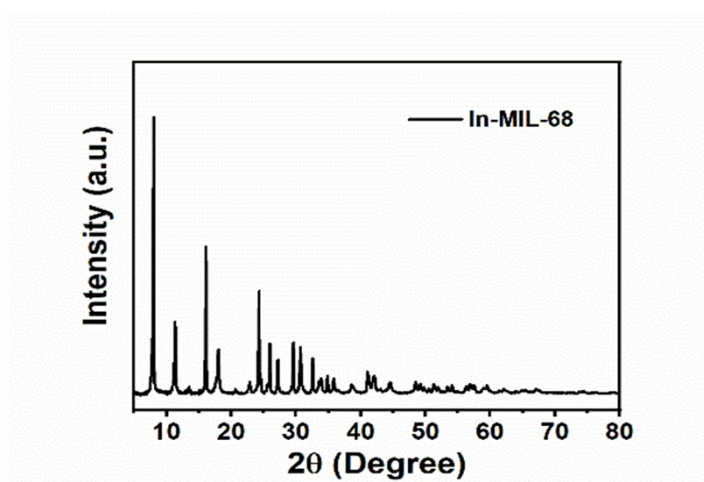
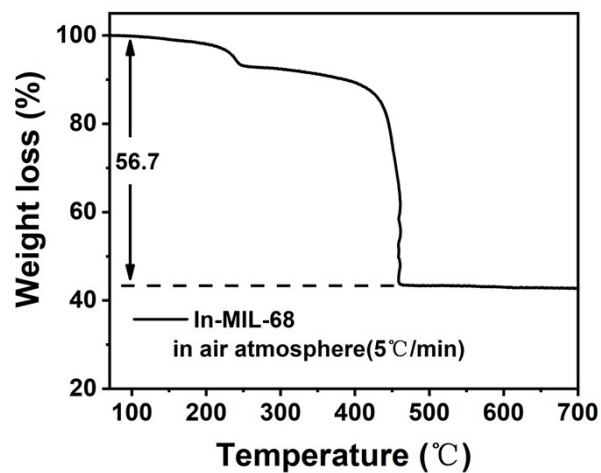
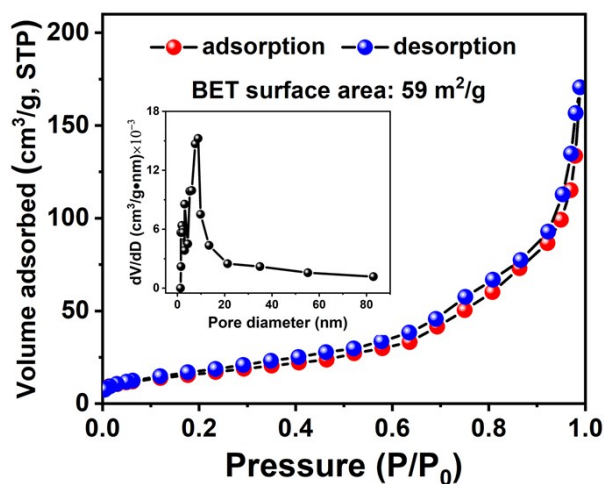


Fig. S1. XRD pattern of In-MIL-68 prisms.



**Fig. S2.** TGA curve of In-MIL-68 prisms in air atmosphere with a heating rate of 5 °C/min.



**Fig. S3.** N<sub>2</sub> sorption isotherms and BET surface area of In<sub>2</sub>O<sub>3</sub>. Inset is the corresponding pore size distribution curve.

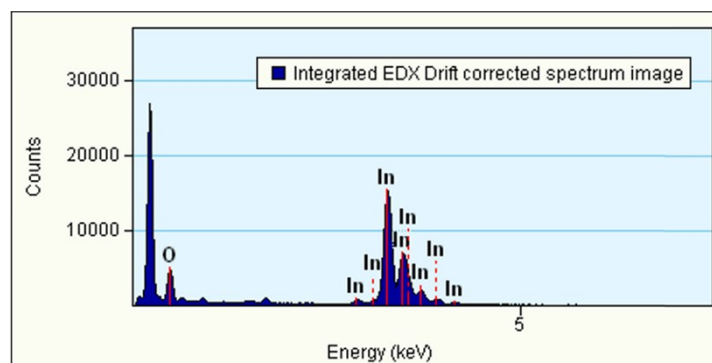


**Fig. S4.** EDX spectrum of In<sub>2</sub>O<sub>3</sub>.

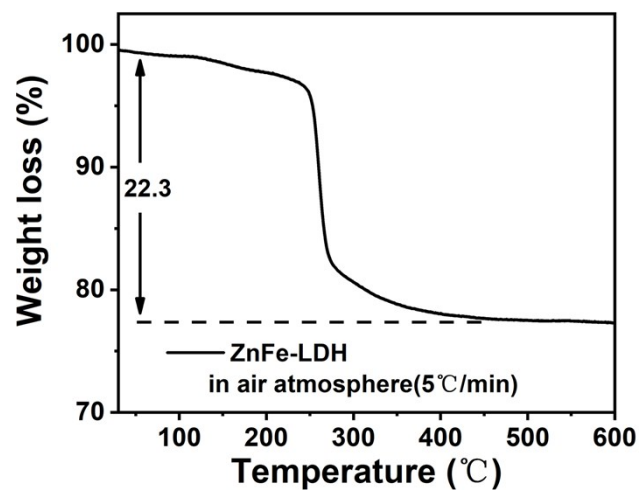


**Fig. S5.** TGA curve of ZnFe-LDH in air atmosphere with a heating rate of 5 °C/min.

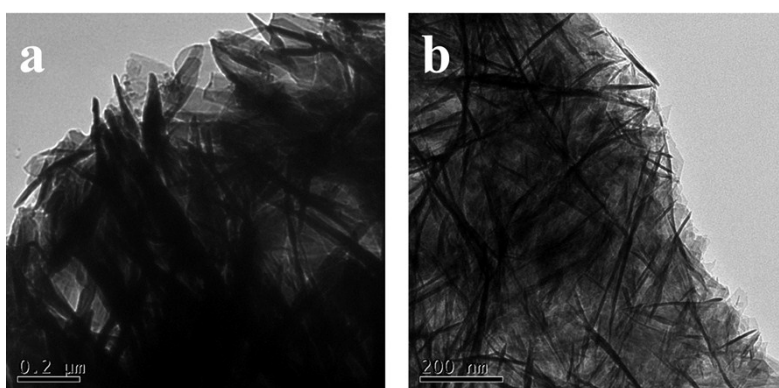


**Fig. S6.** TEM images of (a) ZnFe-LDH and (b) ZnFe<sub>2</sub>O<sub>4</sub>.

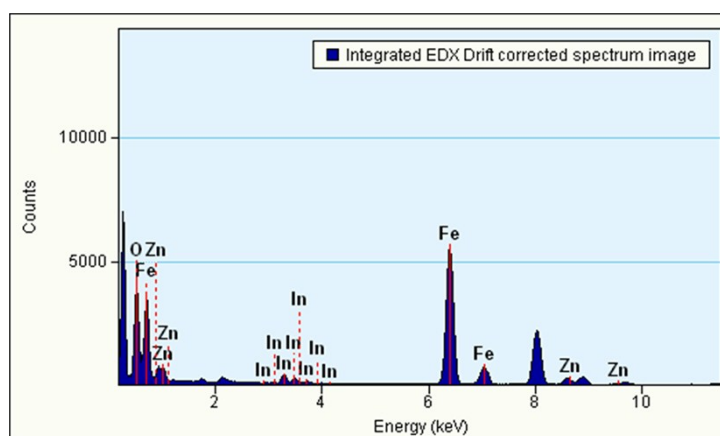


**Fig. S7.** EDX spectrum of In<sub>2</sub>O<sub>3</sub>@ZnFe<sub>2</sub>O<sub>4</sub>-500s.

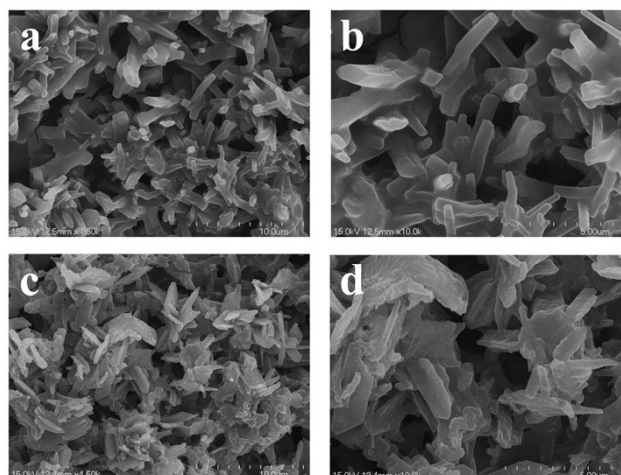


**Fig. S8.** SEM images of (a, b)  $\text{In}_2\text{O}_3@\text{ZnFe}_2\text{O}_4\text{-400s}$ , (c, d)  $\text{In}_2\text{O}_3@\text{ZnFe}_2\text{O}_4\text{-600s}$ .

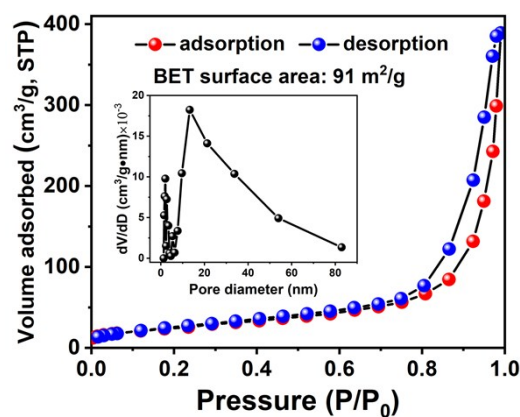


**Fig. S9.**  $\text{N}_2$  sorption isotherms and BET surface area of  $\text{ZnFe}_2\text{O}_4$ . Inset is the corresponding pore size distribution curve.

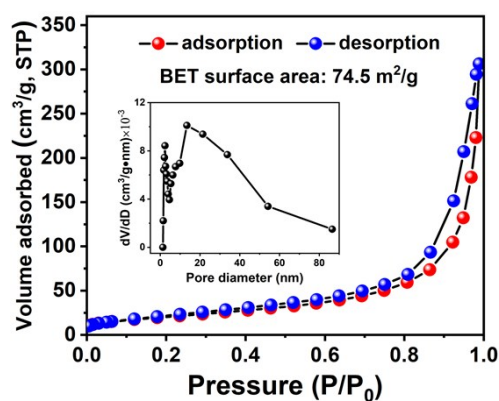


**Fig. S10.**  $\text{N}_2$  sorption isotherms and BET surface area of  $\text{In}_2\text{O}_3@\text{ZnFe}_2\text{O}_4\text{-500s}$ . Inset is the corresponding pore size distribution curve.

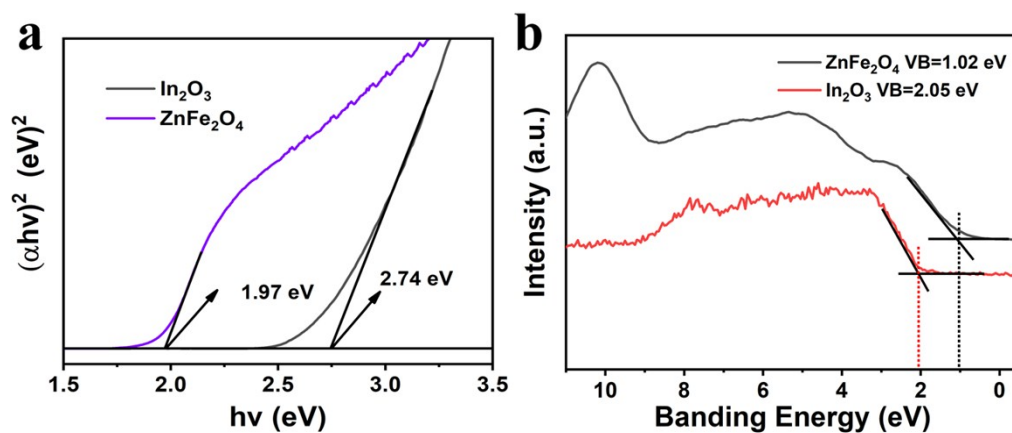


**Fig. S11.** (a) Tauc plots and (b) Valence band XPS spectra of  $\text{In}_2\text{O}_3$  and  $\text{ZnFe}_2\text{O}_4$ .

**Table S1.** The zeta potential and the maximum UV-vis absorption peak ( $\lambda_{\text{max}}$ ) of TC under different pH.

pH	3	5	7	9	11
zeta potential (mV)	12.1	14.7	-1.4	-9.3	-36.2
$\lambda_{\text{max}}$ (nm)	357	357	357	363	377

**Table S2.** Comparison of different contaminants degradation time and efficiency for  $\text{In}_2\text{O}_3@\text{ZnFe}_2\text{O}_4$  with previously reported catalysts.

Photocatalysts	Pollutant	Concentration (mg/L)	Reaction time (min)	Catalyst dosage (g/L)	Removal rate (%)	Ref.
$\text{In}_2\text{O}_3@\text{ZnFe}_2\text{O}_4$	TC	150	60	0.5	90	Our work
Carbon dots/ $\text{MoO}_3/\text{g-C}_3\text{N}_4$	TC	20	90	0.6	88.4	1
$\text{Ag}@\text{g-C}_3\text{N}_4@\text{BiVO}_4$	TC	20	60	0.3	82.75	2
$\text{Ag}_3\text{PO}_4/\text{CuBi}_2\text{O}_4$	TC	20	60	0.5	75	3
type II $\text{AgI}/\text{CuBi}_2\text{O}_4$	TC	10	60	0.5	80	4
Z-scheme $\text{AgBr}/\text{CuBi}_2\text{O}_4$	TC	10	60	0.5	90	4
$\text{Ag}/\text{AgCl}/\text{Bi}_2\text{MoO}_6$	Rhb	10	60	1.0	90.9	5

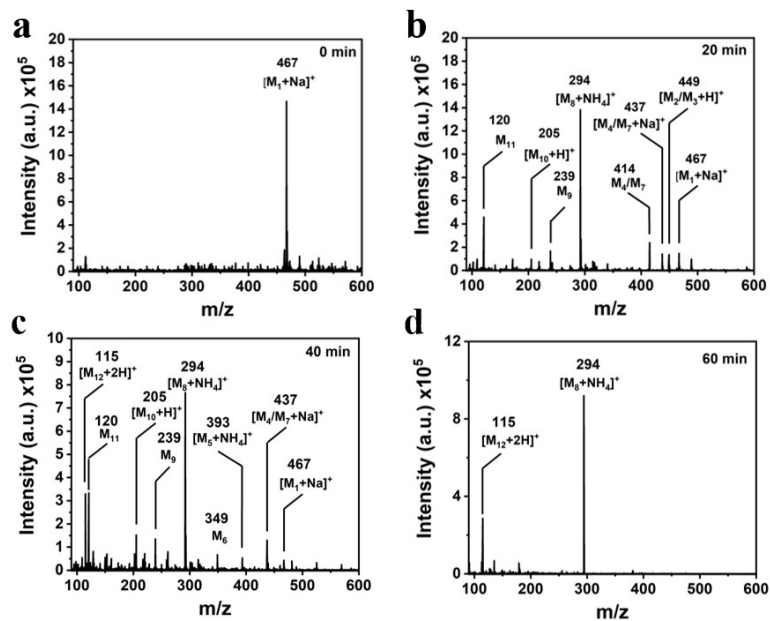


Fig. S12. LC-MS spectra at 0 min (a), 20 min (b), 40 min (c) and 60 min (d).

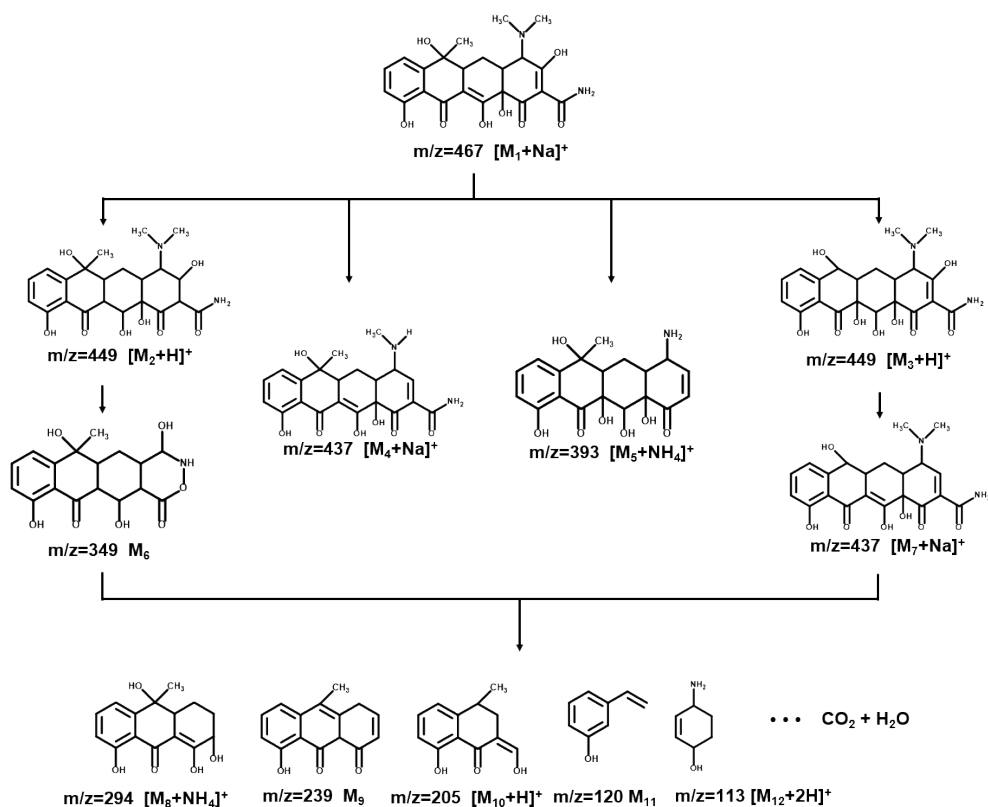
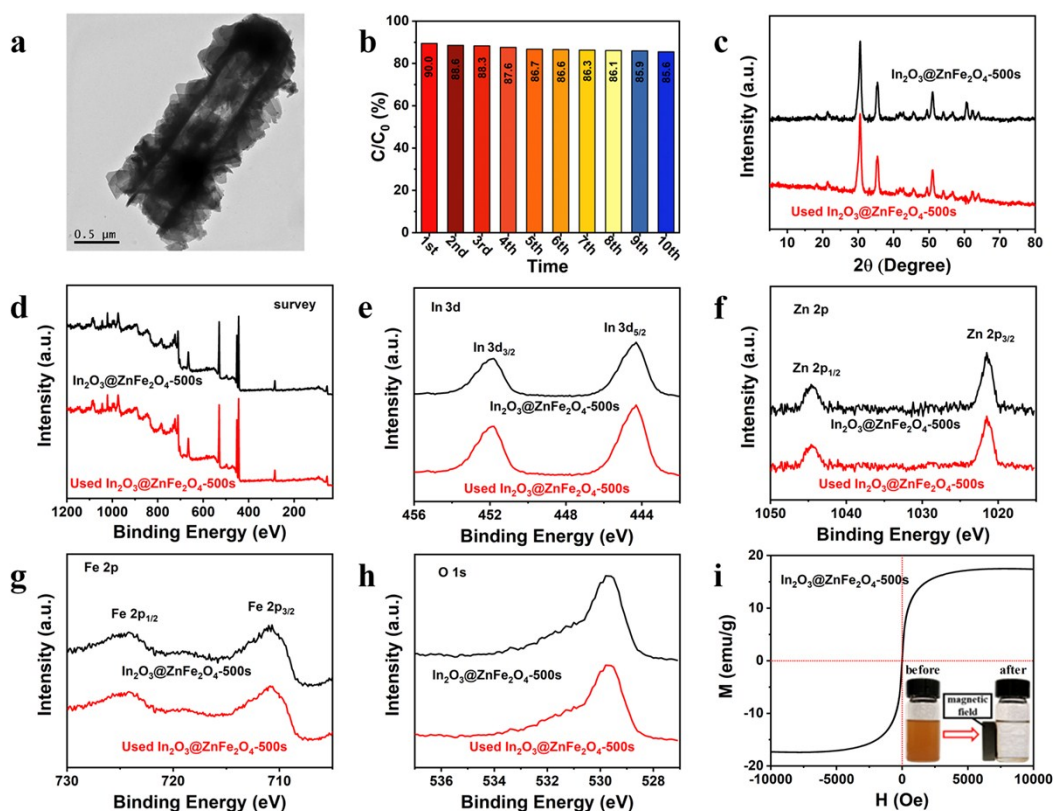


Fig. S13. TC photocatalytic degradation pathway on  $In_2O_3@ZnFe_2O_4$ .



**Fig. S14.** (a). TEM image of  $\text{In}_2\text{O}_3@\text{ZnFe}_2\text{O}_4-500\text{s}$  after photocatalytic process. (b). Cycling runs for the degradation of TC (pH=11, TC=50 mg/L,  $\text{In}_2\text{O}_3@\text{ZnFe}_2\text{O}_4-500\text{s}$  = 0.5 g/L), (c). XRD patterns and XPS spectra of  $\text{In}_2\text{O}_3@\text{ZnFe}_2\text{O}_4-500\text{s}$  before and after 10 times photocatalytic reactions: (d) survey, (e) In 3d, (f) Zn 2p, (g) Fe 2p and (h) O 1s, (i). Magnetic hysteresis loop of  $\text{In}_2\text{O}_3@\text{ZnFe}_2\text{O}_4-500\text{s}$  (insert: the solution before and after magnetic separation).

## References

1. Z. Xie, Y. Feng, F. Wang, D. Chen, Q. Zhang, Y. Zeng, W. Lv and G. Liu, Construction of carbon dots modified  $\text{MoO}_3/\text{g-C}_3\text{N}_4$  Z-scheme photocatalyst with enhanced visible-light photocatalytic activity for the degradation of tetracycline, *Applied Catalysis B: Environmental*, 2018, **229**, 96-104.
2. F. Chen, Q. Yang, Y. Wang, J. Zhao, D. Wang, X. Li, Z. Guo, H. Wang, Y. Deng, C. Niu and G. Zeng, Novel ternary heterojunction photocatalyst of Ag nanoparticles and g-C<sub>3</sub>N<sub>4</sub> nanosheets co-modified BiVO<sub>4</sub> for wider spectrum visible-light photocatalytic degradation of refractory pollutant, *Applied Catalysis B: Environmental*, 2017, **205**, 133-147.
3. W. Shi, F. Guo and S. Yuan, In situ synthesis of Z-scheme  $\text{Ag}_3\text{PO}_4/\text{CuBi}_2\text{O}_4$  photocatalysts and enhanced photocatalytic performance for the degradation of tetracycline under visible light irradiation, *Applied Catalysis B: Environmental*, 2017, **209**, 720-728.

4. F. Guo, W. Shi, H. Wang, M. Han, W. Guan, H. Huang, Y. Liu and Z. Kang, Study on highly enhanced photocatalytic tetracycline degradation of type II AgI/CuBi<sub>2</sub>O<sub>4</sub> and Z-scheme AgBr/CuBi<sub>2</sub>O<sub>4</sub> heterojunction photocatalysts, *Journal of Hazardous Materials*, 2018, **349**, 111-118.
5. J. Zhang, C. Niu, J. Ke, L. Zhou and G. Zeng, Ag/AgCl/Bi<sub>2</sub>MoO<sub>6</sub> composite nanosheets: A plasmonic Z-scheme visible light photocatalyst, *Catalysis Communications*, 2015, **59**, 30-34.